NACA RM A51F12a

NACA

# RESEARCH MEMORANDUM

## INVESTIGATION OF A TRIANGULAR WING IN CONJUNCTION WITH A FUSELAGE AND HORIZONTAL TAIL TO DETERMINE DOWNWASH AND LONGITUDINAL-STABILITY CHARACTERISTICS - TRANSONIC BUMP METHOD

By Edwin C. Allen

Ames Aeronautical Laboratory
Moffett Field, Calif.



NATIONAL ADVISORY COMMITTEE
FOR AERONAUTICS

WASHINGTON

August 17, 1951

NATIONAL ADVISORY COMMITTEE FOR AERONAUTICS

RESEARCH MEMORANDUM

# INVESTIGATION OF A TRIANGULAR WING IN CONJUNCTION WITH A FUSELAGE AND HORIZONTAL TAIL TO DETERMINE DOWNWASH AND LONGITUDINAL-STABILITY CHARACTERISTICS - TRANSONIC BUMP METHOD

By Edwin C. Allen

## SUMMARY

The results are presented of an experimental investigation of the downwash and longitudinal-stability characteristics of a semispan, triangular-wing, airplane model with a horizontal tail. Transonic speeds were obtained by using the transonic bump in the Ames 16-foot high-speed wind tunnel. The model consisted of a thin triangular wing having an aspect ratio of 2, with a fuselage having a fineness ratio of 12.5, and a thin unswept horizontal tail having an aspect ratio of 4. Tests were made with the horizontal tail in the wing-chord plane extended and also 0.25 wing semispan above and below the wing-chord plane, all at one longitudinal station behind the wing. The Mach number range was 0.40 to 1.10 with a corresponding Reynolds number range of 1.0 to 1.9 million. The lift, drag, and pitching-moment data are presented for the wing-fuselage combination. Also the pitching-moment data for the wing, fuselage, and horizontal-tail combination are presented. The effective downwash at the tail is obtained from a comparison of these results.

The results of the tests indicate that the model with the tail on or below the wing-chord plane possessed satisfactory stability characteristics throughout the test range of lift coefficient. The model with the tail above the wing-chord plane possessed undesirable stability characteristics due to large variations of downwash at the higher lift coefficients.

## INTRODUCTION

Studies have been made of the flow fields behind wings of low aspect ratio at both subsonic and supersonic speeds. However, there has been little investigation of the flow fields behind low-aspect-ratio wings at transonic speeds.

The purpose of this investigation was to determine the longitudinal-stability characteristics of and the effective downwash at one position behind a triangular-wing model at transonic speeds, using the transonic bump in the Ames 16-foot high-speed wind tunnel. The tests were conducted in conjunction with the investigation of the low-speed characteristics of the same configuration in the Ames 40- by 80-foot wind tunnel. The model was tested with three vertical positions of the horizontal tail.

## NOTATION

$C_D$ drag coefficient $\left(\frac{\text{twice drag of half model}}{qS}\right)$

$C_L$ lift coefficient $\left(\frac{\text{twice lift of half model}}{qS}\right)$

$C_m$ pitching-moment coefficient about quarter point of the wing mean aerodynamic chord $\left(\frac{\text{twice pitching moment of half model}}{qS\bar{c}}\right)$

$M$ free-stream Mach number

$M_L$ local Mach number

$S$ twice wing area of half model, square feet

$V$ free-stream velocity, feet per second

$b$ wing span feet

$c$ local wing chord, feet

$\bar{c}$ wing mean aerodynamic chord $\left(\frac{\int_0^{b/2} c^2\,dy}{\int_0^{b/2} c\,dy}\right)$, feet

$i_t$ horizontal-tail incidence angle with respect to wing-chord plane, degrees

$q$ dynamic pressure $\left(\frac{1}{2}\rho V^2\right)$, pounds per square foot

$y$ spanwise distance from plane of symmetry, feet

$\alpha$ wing angle of attack, degrees

$\epsilon$ effective downwash angle, degrees

$\rho$ mass density of air, slugs per cubic foot

## APPARATUS

### Wind Tunnel and Equipment

The tests were conducted on the transonic bump of the Ames 16-foot high-speed wind tunnel. The bump is described in detail in reference 1. The aerodynamic forces and moments were measured by means of a strain-gage balance mounted inside the bump. The wing-flow balance described in reference 2 was used.

### Model

A three-view drawing of the model is shown in figure 1 and photographs of the model mounted on the bump are shown in figure 2.

The wing of the model, identical in proportion to the semispan of the wing described in reference 3, had an aspect ratio of 2. The airfoil sections parallel to the model center line were the modified NACA 0005. The fuselage was of circular cross section and had a fineness ratio of 12.5. For a more complete model description, see reference 3.

The horizontal tail had an aspect ratio of 4, taper ratio of 0.5, and the 0.50-chord line was unswept. The basic 4.5-percent-thick diamond profile was modified by rounding the ridge for a distance of 15 percent of the local chord, resulting in a thickness-to-chord ratio of 0.042. The tail was attached to the fuselage by a rigid beam beneath the reflection plate so as to transfer all loads applied on the tail through the fuselage and then to the balance. The tail incidence was limited to $\pm 5^\circ$ with the tail on the wing-chord plane extended.

The model was tested in the presence of a reflection plate as shown in figures 1 and 2. The reflection plate was mounted independently of the model, thereby separating aerodynamic loads on the plate from the measured forces and moments.

## TESTS AND PROCEDURES

Force and moment data were obtained for the model with the horizontal tail at each of the three vertical positions and with the horizontal tail off. The tests were made over a Mach number range of 0.40 to 1.10 with a corresponding Reynolds number range of 1.0 to 1.9 million, based on the wing mean aerodynamic chord. (See fig. 3.)

The model was mounted in a local, high-velocity region on the transonic bump. Typical contours of local Mach number in the bump flow field (with the model removed) are shown in figure 4. The outline of the model has been superimposed on these contours to indicate the Mach number gradients which existed in the region of the model. No attempt has been made to evaluate the effects of these gradients. The free-stream Mach numbers presented in this report are the average Mach numbers in the region of the wing of the model.

An angle-of-attack correction of $-0.7^\circ$ was included due to the angularity of flow over the bump. There was believed to be a slight variation of the flow angularity (of the order of $0.5^\circ$) along the length of the model. Since this variation could not be determined accurately, the flow angularity was assumed to be constant for the length of the model.

The absolute values of the drag coefficients presented are not believed to be entirely reliable because of the shortcoming inherent in the balance which resulted in a drag reading when a lift force was applied. For this reason the drag coefficients were not corrected for the flow angularity over the bump. However, the drag coefficients are of qualitative interest in that they show the order of magnitude of the changes in drag throughout the transonic Mach number range.

## RESULTS AND DISCUSSION

### Aerodynamic Characteristics of the Wing-Fuselage Combination

The effects of Mach number on the force and moment characteristics of the wing-fuselage combination are presented in figure 5. The forces and moments changed gradually with Mach number, the most notable change

being a 20-percent increase of maximum lift at transonic speeds. The lift-curve slope and minimum-drag coefficient increased with Mach number while the pitching-moment curves indicated increased static longitudinal stability and became more nearly linear at the higher Mach numbers.

The effective downwash behind the wing was measured by inserting the horizontal tail at various angles of incidence in the flow field of the wing and measuring the total pitching moments of the complete model (figs. 6, 7, and 8). The lift and, consequently, the angle of attack of the tail, were assumed to be zero when the moment with the tail on was equal to the moment with the tail off. The effective downwash at the tail, at the angles of attack and tail incidences where the tail-on and tail-off moment curves intersect, was then calculated by the relation $\epsilon = \alpha + i_t$. The variation of this downwash angle with angle of attack is presented in figure 9 for the three tail heights tested. The slight angle of downwash indicated for $0^\circ$ angle of attack when the horizontal tail was on the wing-chord plane is believed to be due to the variation of flow angularity over the bump from the wing to the tail position.

In order to present a clearer concept of the effect of the downwash on the longitudinal stability, the rates of change of downwash angle with angle of attack for the three tail heights are compared in figure 10. It should be noted that the downwash variations shown appear somewhat erratic. However, calculations of downwash from the increment of pitching moment due to a fixed setting of the tail (using an average value for $dC_m/di_t$) resulted in similar erratic variations. Thus, the possibility of the erratic variations being caused by errors which were not consistent for the various horizontal-tail settings is eliminated. Examination of the figure shows a marked change of $d\epsilon/d\alpha$ with vertical position. Below the wing-chord plane the downwash was such that a tail would generally be more stabilizing than for either of the other two positions. For the position above the wing-chord plane, and angles of attack between about $7^\circ$ and $14^\circ$, the rate of change of downwash with angle of attack was greater than 1.0, indicating that a tail placed here would be destabilizing. The variations in downwash with vertical position are believed to be due to the separation-vortex type of flow known to exist on low-aspect-ratio, thin triangular wings. (See references 3 and 4.)

## Aerodynamic Characteristics of the Wing, Fuselage, and Horizontal-Tail Combination

The pitching-moment characteristics of the model with the tail at $0^\circ$ incidence in each of the three positions are presented in figure 11. With the tail above the wing-chord plane the model was stable through

the low lift-coefficient range, became unstable to marginally stable through the middle of the lift-coefficient range, and then became stable again near the highest lift coefficients. With the tail on or below the wing-chord plane the model was stable throughout the test range of lift coefficient. This result is in agreement with what would be expected from examination of the wing-body pitching moments in figure 5 and the downwash characteristics shown in figures 9 and 10, assuming linear lift characteristics of the tail. Examination of figures 6, 7, and 8 indicates that the pitching-moment characteristics of the model for $0^\circ$ tail incidence are typical of those for the other tail incidences.

## CONCLUDING REMARKS

Results of the tests of the model show that, with the tail on or one-fourth wing semispan below the wing-chord plane, the model possessed satisfactory static longitudinal stability throughout the test range of lift coefficient and Mach number. With the tail one-fourth wing semispan above the wing-chord plane the model had undesirable static longitudinal-stability characteristics at moderate lift coefficients, due to the large rate of change of downwash with angle of attack at this position.

Ames Aeronautical Laboratory,
National Advisory Committee for Aeronautics,
Moffett Field, Calif.

## REFERENCES

1. Axelson, John A., and Taylor, Robert A.: Preliminary Investigation of the Transonic Characteristics of an NACA Submerged Inlet. NACA RM A50C13, 1950.

2. Rathert, George A., Jr., Hanson, Carl M., and Rolls, L. Stewart: Investigation of a Thin Straight Wing of Aspect Ratio 4 by the NACA Wing-Flow Method.- Lift and Pitching-Moment Characteristics of the Wing Alone. NACA RM A8L20, 1949.

3. Graham, David, and Koenig, David G.: Tests in the Ames 40- by 80-Foot Wind Tunnel of an Airplane Configuration With an Aspect Ratio 2 Triangular Wing and an All-Movable Horizontal Tail - Longitudinal Characteristics, NACA RM A51B21, 1951.

4. Perkins, Edward W., and Canning, Thomas N.: Investigation of Downwash and Wake Characteristics at a Mach Number of 1.53. II – Triangular Wing. NACA RM A9D20, 1949.

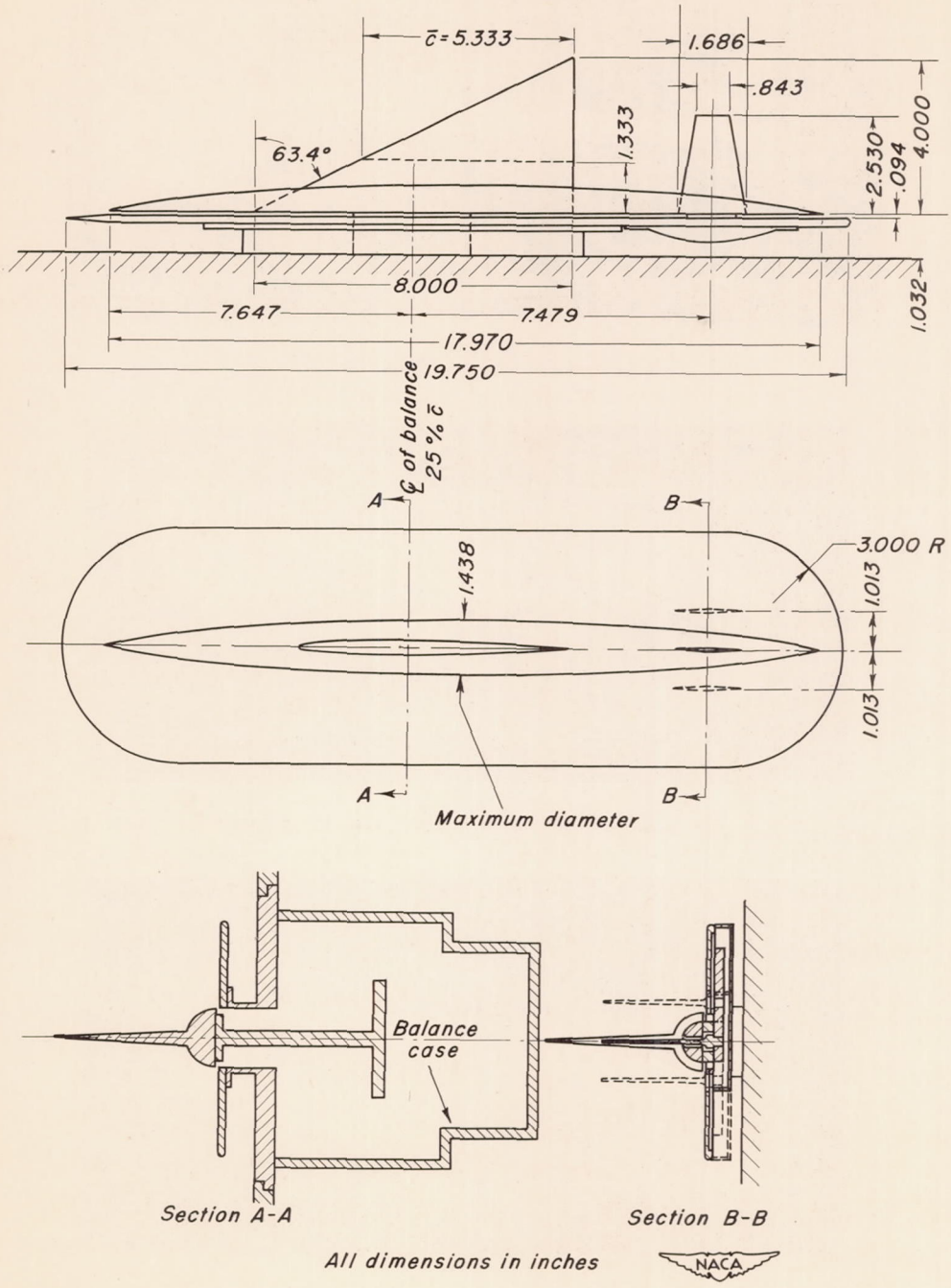


Figure 1.- Schematic drawing of the model.

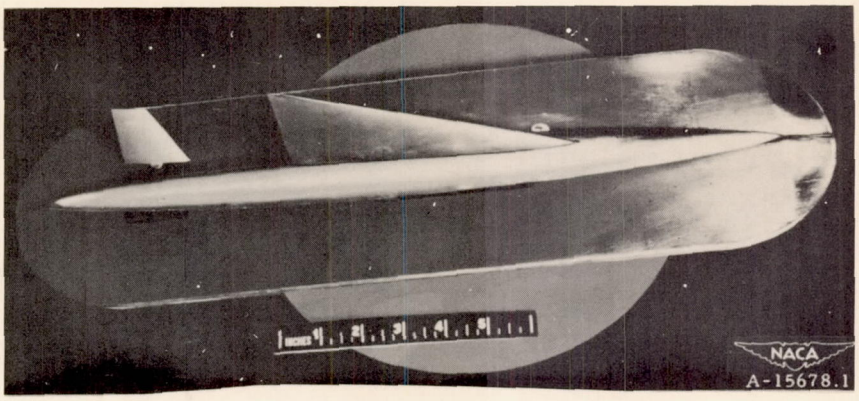


(a) Tail above the wing–chord plane.

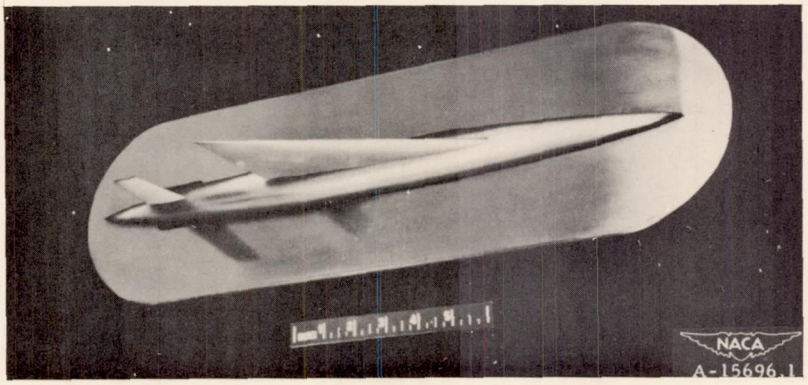


(b) Tail on the wing–chord plane.

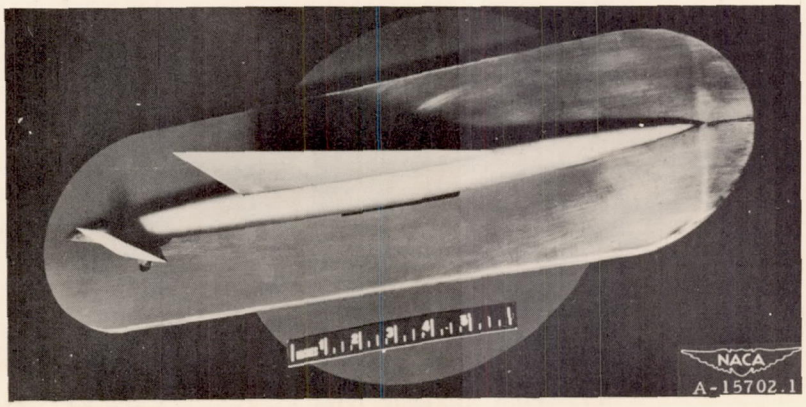


(c) Tail below the wing–chord plane.

Figure 2.– Models mounted on the transonic bump showing the three horizontal–tail positions tested.

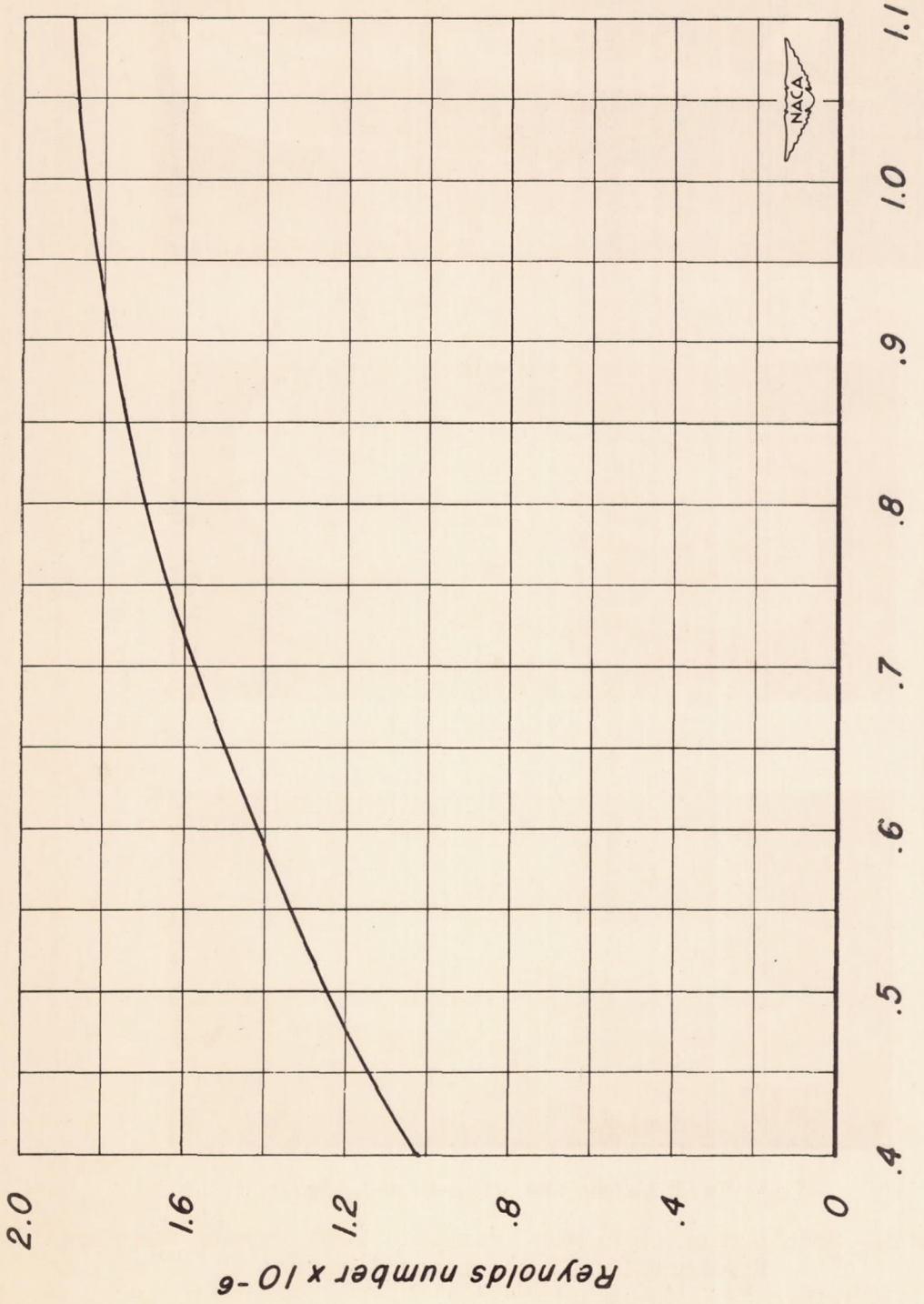


Figure 3.- Variation of test Reynolds number with Mach number.

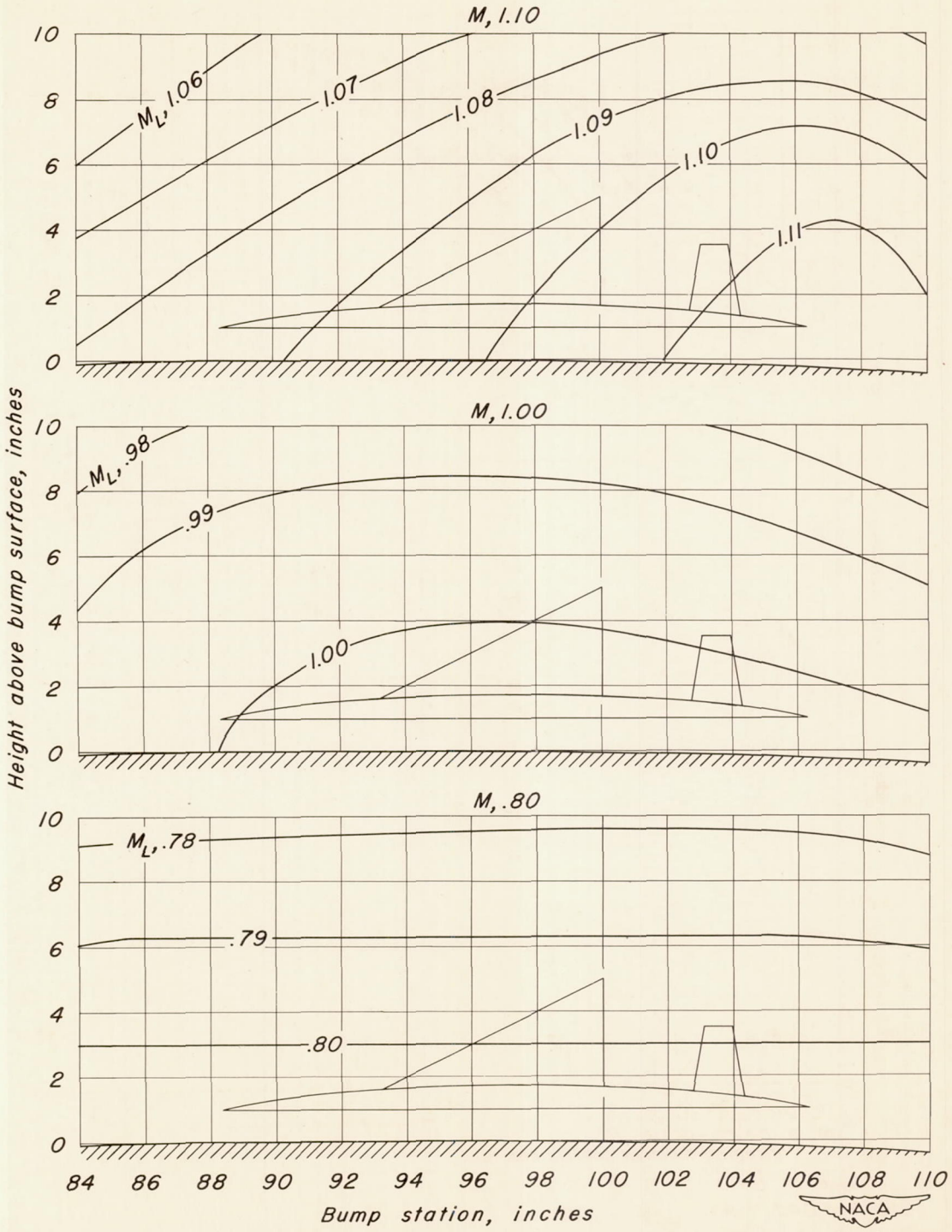


*Figure 4.- Typical Mach-number contours over the transonic bump in the Ames 16-foot high-speed wind tunnel.*

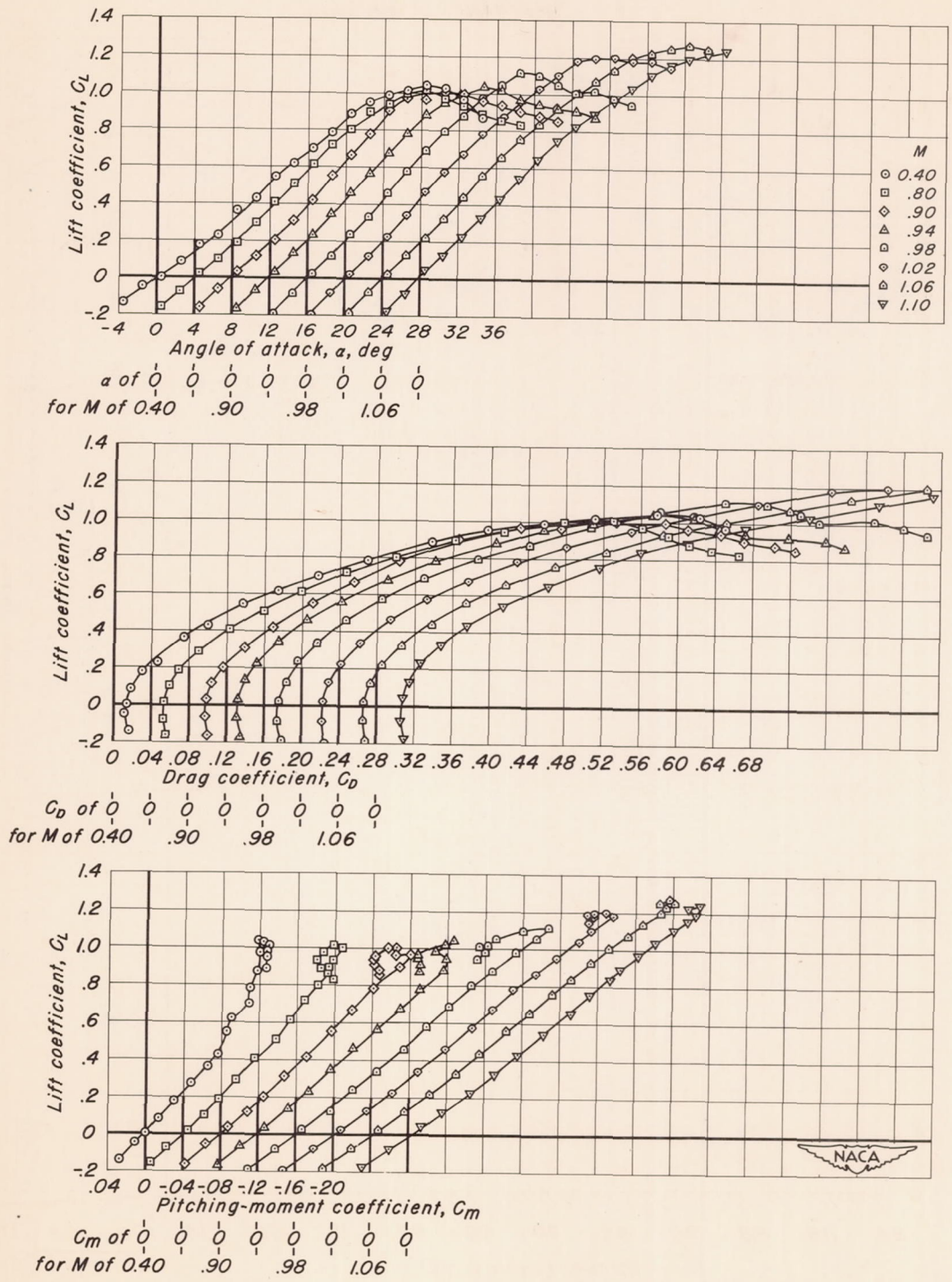


*Figure 5.- The effects of Mach number on the aerodynamic characteristics of the wing-fuselage combination.*

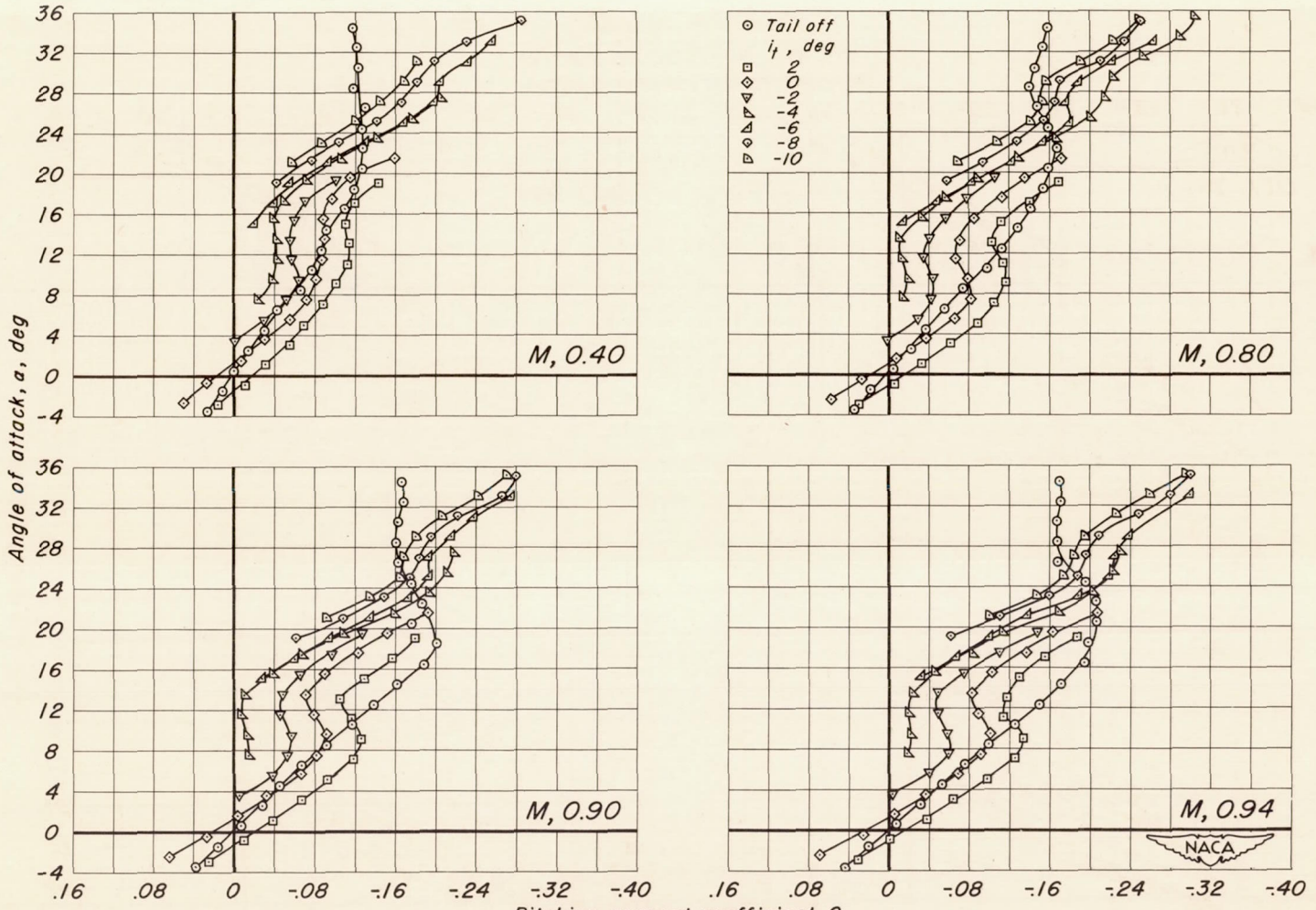


(a) M, 0.40, 0.80, 0.90, and 0.94.

Figure 6.- The effects of the horizontal-tail incidence on the pitching-moment characteristics, tail above the wing-chord plane.

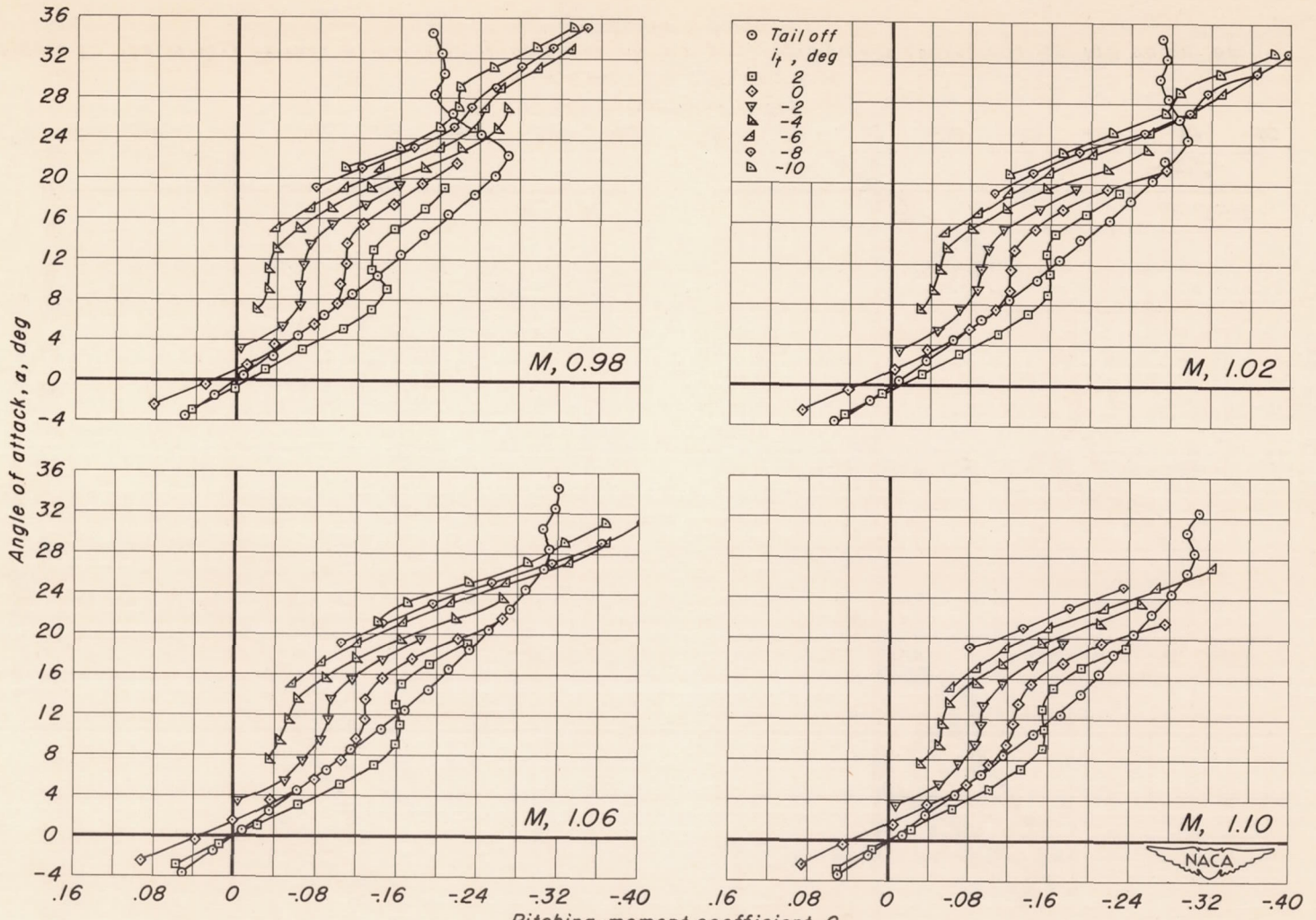


(b) M, 0.98, 1.02, 1.06, and 1.10.

Figure 6.- Concluded.

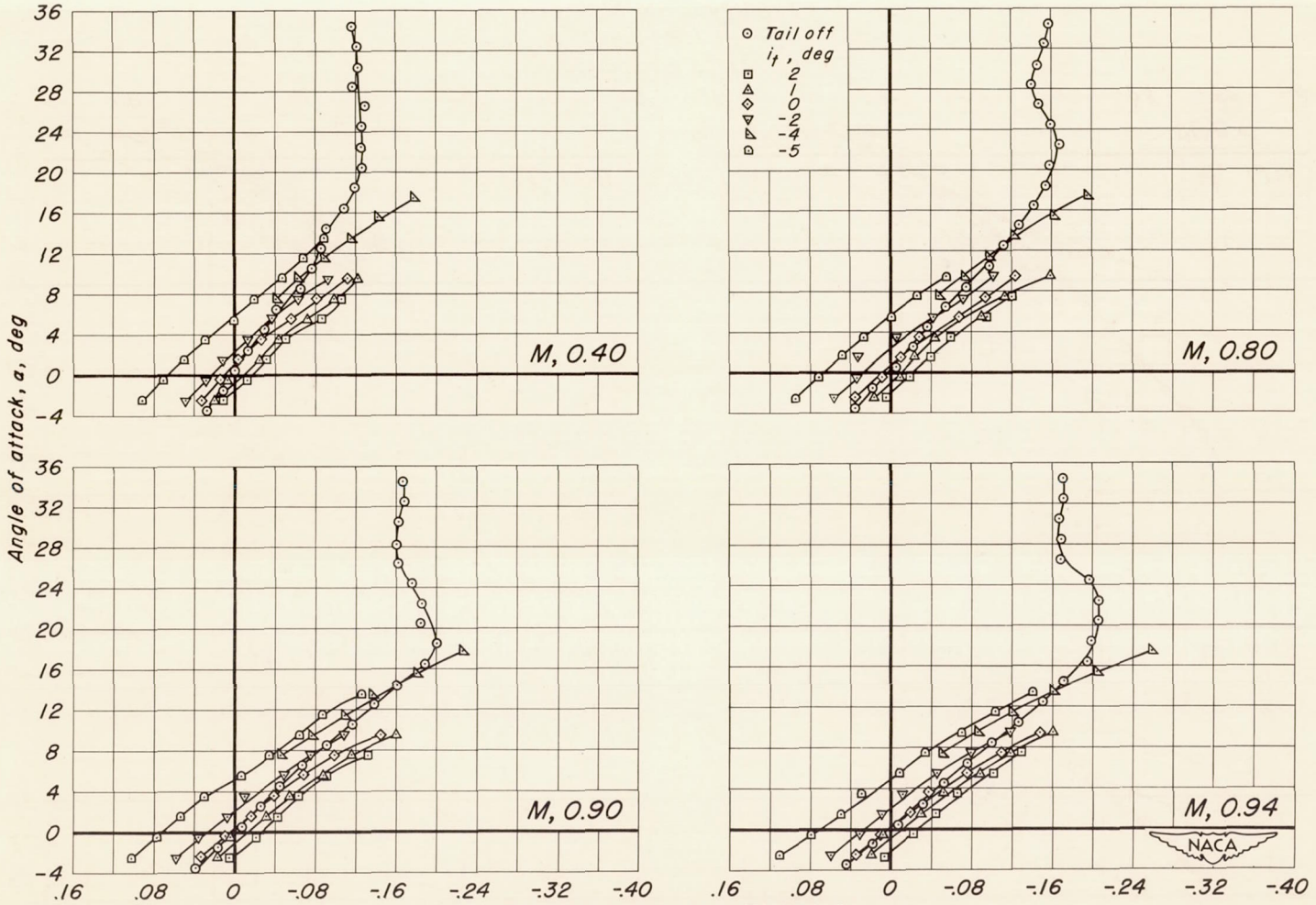


(a) M, 0.40, 0.80, 0.90, and 0.94.

*Figure 7.- The effects of the horizontal-tail incidence on the pitching-moment characteristics, tail on the wing-chord plane.*

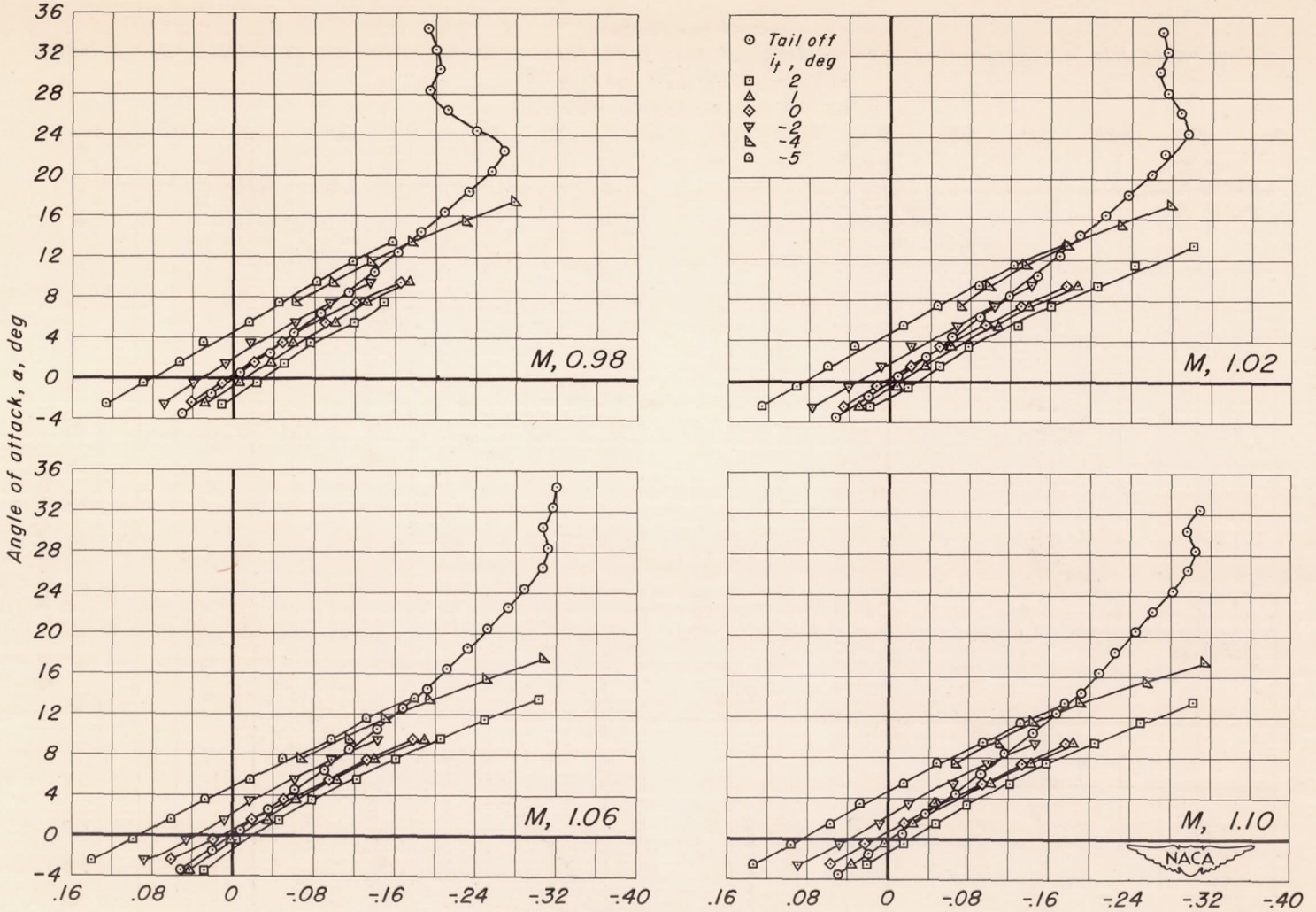


(b) M, 0.98, 1.02, 1.06, and 1.10.

Figure 7.- Concluded.

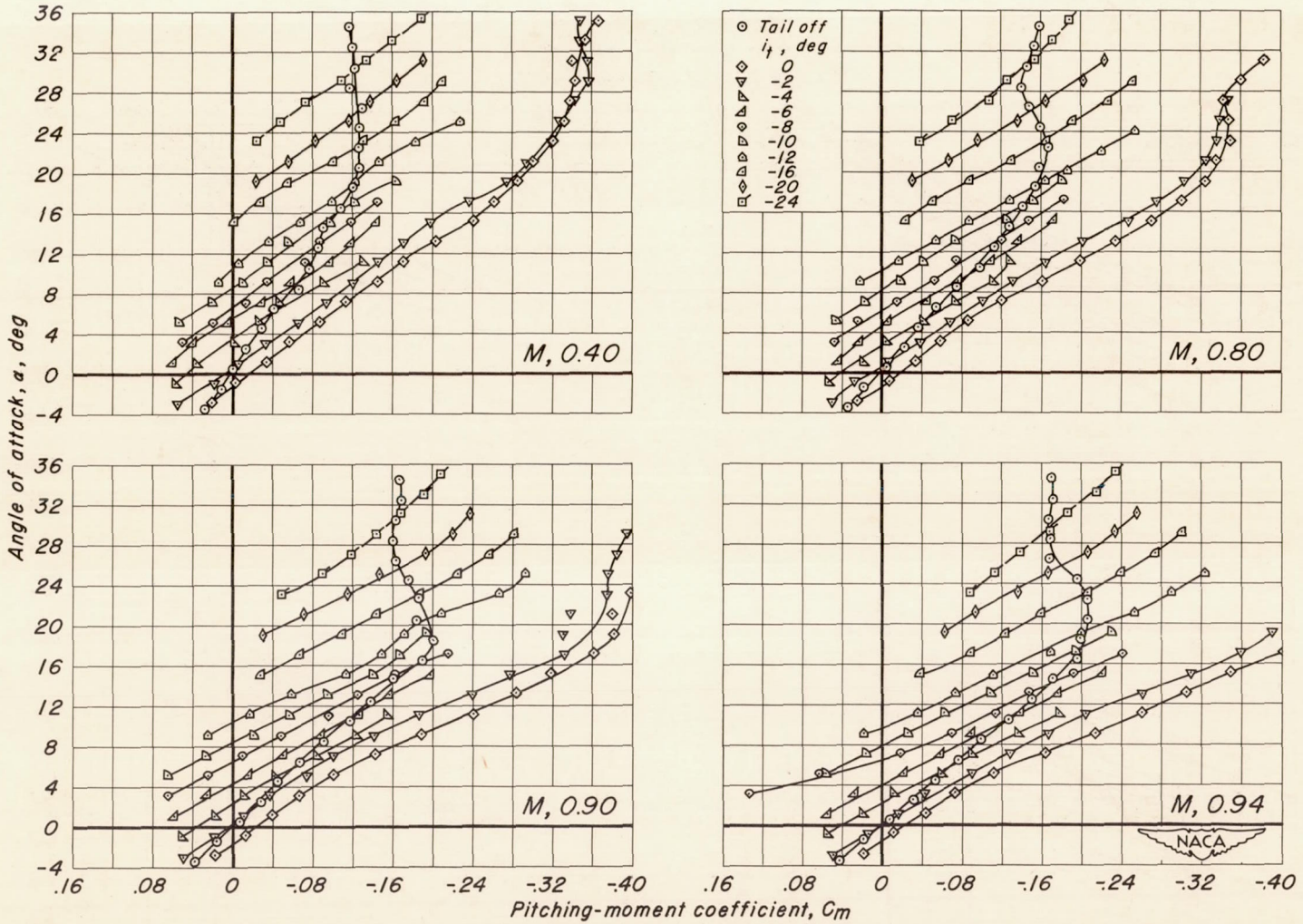


(a) M, 0.40, 0.80, 0.90, and 0.94.

*Figure 8.- The effects of the horizontal-tail incidence on the pitching-moment characteristics, tail below the wing-chord plane.*

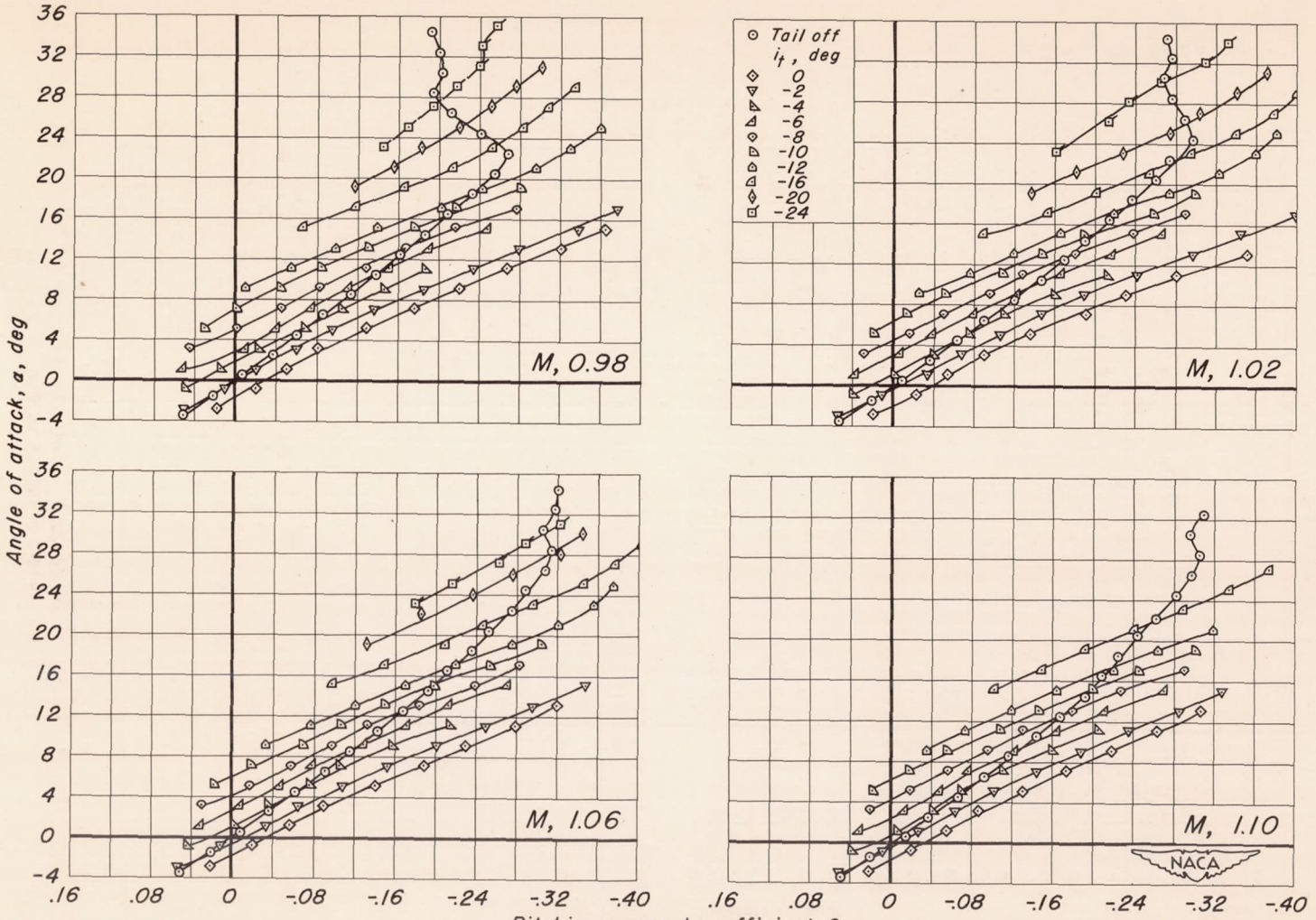


(b) M, 0.98, 1.02, 1.06, and 1.10.

Figure 8.- Concluded.

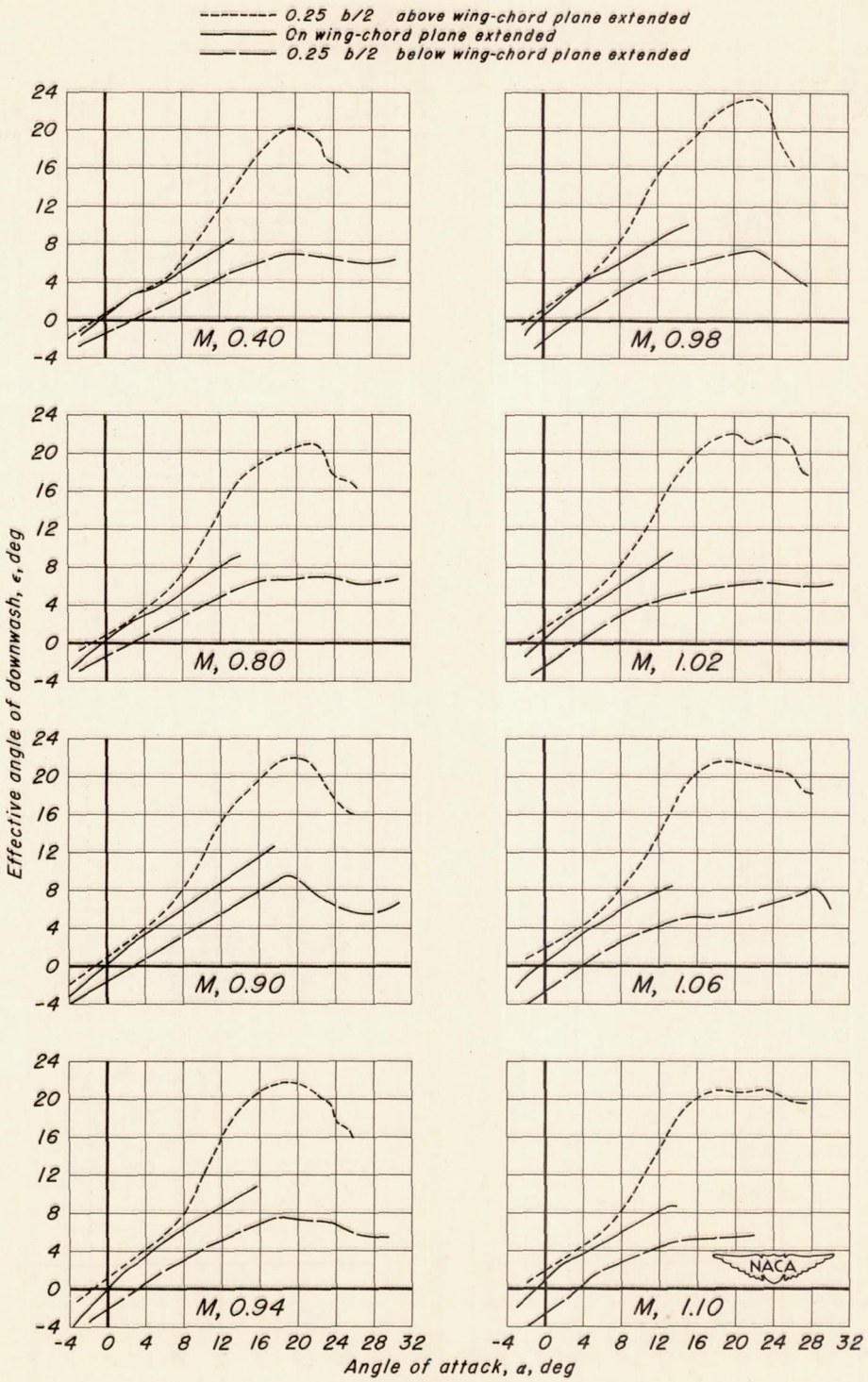


Figure 9.- Variation of downwash with angle of attack.

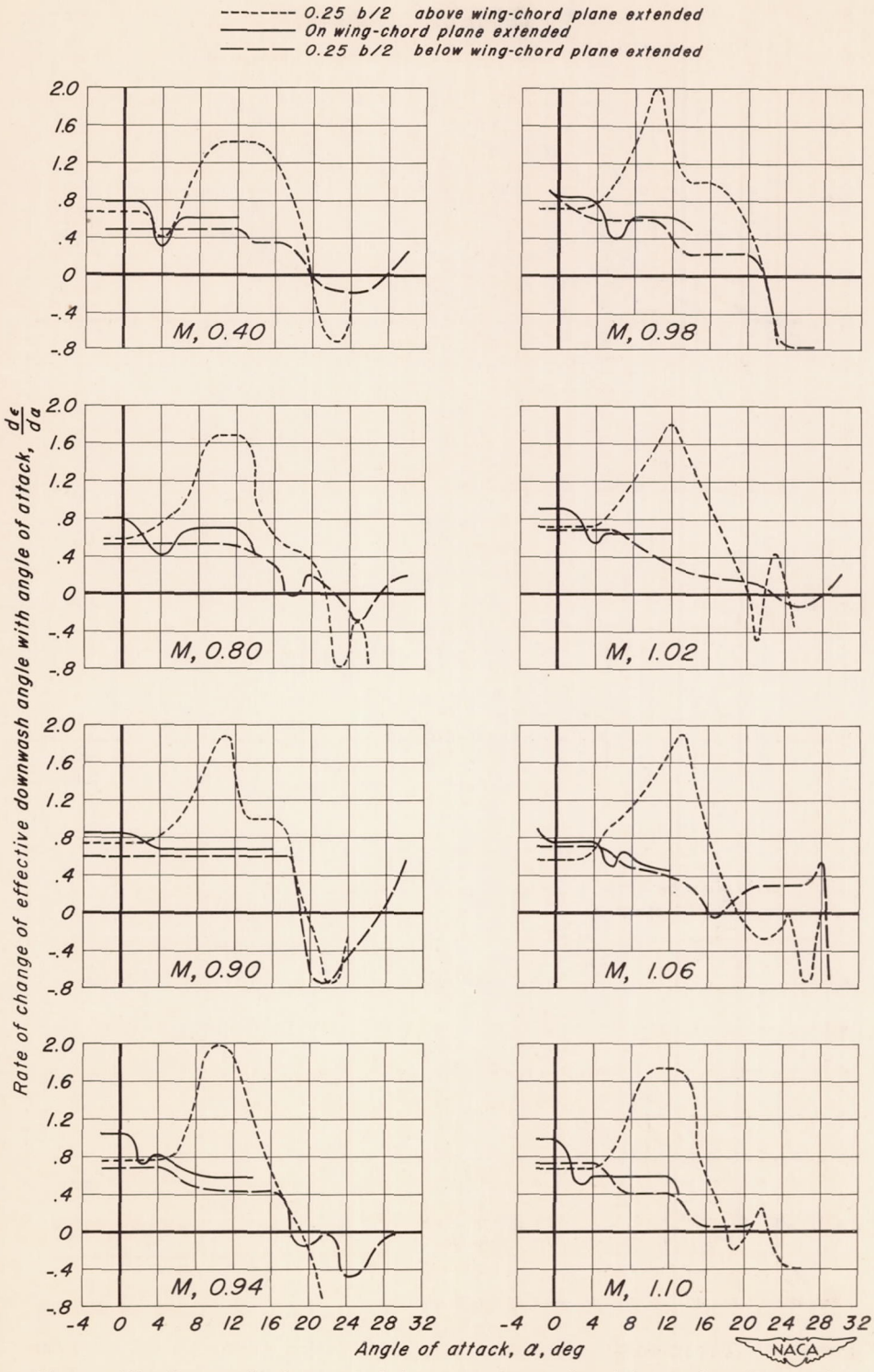


Figure 10.- Rate of change of downwash angle with angle of attack.

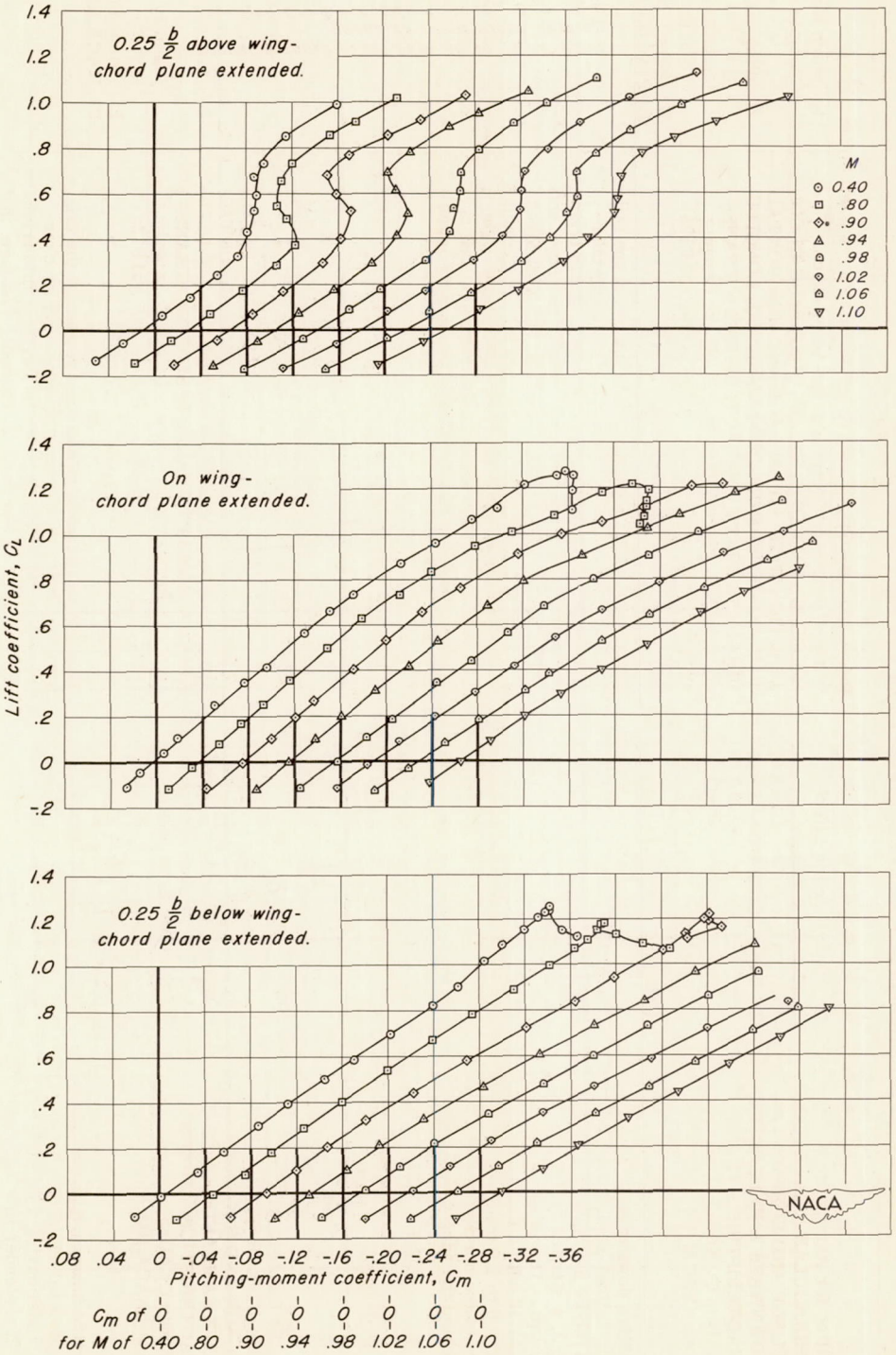


*Figure 11.— The pitching-moment characteristics of the model with the tail in each of the three positions. $i_t$, 0°.*